Available online at www.sciencedirect.com
SCIENCE DIRECT®
Pergamon
Cement and Concrete Research 33 (2003) 835–840
CEMENT AND CONCRETE RESEARCH

The origin of nonlinear current–voltage behavior in fiber-reinforced cement composites

A.D. Hixson, L.Y. Woo, M.A. Campo, T.O. Mason*

Department of Materials Science and Engineering, Northwestern University, 2225 North Campus Drive, Evanston, IL 60208, USA

Received 23 January 2001; accepted 22 November 2002

Abstract

Two distinct slopes (resistances) are obtained in current–voltage (I–V) plots of discontinuous, conductive fiber-reinforced cement composites. The low-field resistance correlates with the DC resistance (R_{DC}) of each composite. The high-field resistance correlates with the intermediate frequency cusp resistance (R_{cusp}) in Nyquist ($-Z_{imag}$ vs. Z_{real}) plots obtained using impedance spectroscopy (IS). A model is developed that is based on passive oxide film formation on copper or steel fiber surfaces at low fields (I–V) or low frequencies (IS) due to the high pH pore solution of cement paste. With increase of field, leading to film breakdown (active or transpassive corrosion behavior), or increase of frequency, leading to short-circuiting of the passive layer, the fibers act as short-circuiting elements in the composite microstructure, resulting in a decrease in overall resistance.

Keywords: Electrical properties; Electrochemical properties; Reinforcement; Portland cement; Composite

1. Introduction

Nonlinear current–voltage (I–V) behavior is common in semiconductor-based junctions and in heterogeneous ceramics [1]. In the case of grain boundary-controlled (GBC) electroceramics, separate impedance arcs are obtained in Nyquist plots ($-Z_{imag}$ vs. Z_{real}), one corresponding to the resistive grain boundaries and one corresponding to the more conductive grain cores [2]. I–V plots can be highly nonlinear, e.g., in varistors, with a several order-of-magnitude increase in current when field above a certain threshold voltage is applied [3]. There is an excellent correlation between the I–V slopes above and below the transition and the corresponding arc diameters (resistances) in impedance Nyquist plots. Nonlinear electroceramics find applications in surge protection (varistors) and temperature-sensing/switching (thermistors).

Recently, Wen and Chung reported nonlinear I–V behavior in carbon fiber-reinforced cement composites [4]. Their results were similar to those of the present study presented in Fig. 1, showing symmetrical two-slope behavior. At low fields, the I–V slope corresponds to the inverse of the DC resistance (R_{DC}) of the specimen. Above a threshold voltage, approximately the same in forward vs. reverse bias, there is a transition to a higher slope (lower resistance) behavior. This behavior is in marked contrast to that of fiber-free cement paste specimens, which exhibit a single I–V slope corresponding to the inverse of DC resistance (see below). Wen and Chung [4] suggested that conductive fiber-reinforced cement-based materials could be used for temperature-sensing, based on the temperature dependence of resistivity.

Given the well-established correlation between impedance spectroscopy (IS) and I–V behavior in electroceramics, the present work undertook both measurements on conductive fiber/cement–matrix composites. It was recently demonstrated that cement pastes with short conductive fiber additions exhibit dual-arc Nyquist plots ($-Z_{imag}$ vs. Z_{real}) and a ‘‘frequency-switchable coating’’ model was proposed to explain the behavior [5–7]. A highly resistive passive oxide film, known to form on copper or steel surfaces at high pH [8–11], effectively insulates the fibers from the matrix at DC and low AC frequencies. At intermediate frequencies, however, displacement currents through the film short out the oxide coating and the fibers become short-circuit current paths in the matrix. It is well known that high DC fields can

* Corresponding author. Tel.: +1-847-491-3198; fax: +1-847-491-7820.
E-mail address: t-mason@northwestern.edu (T.O. Mason).

0008-8846/02/$ – see front matter © 2002 Elsevier Science Ltd. All rights reserved.
doi:10.1016/S0008-8846(02)01062-1

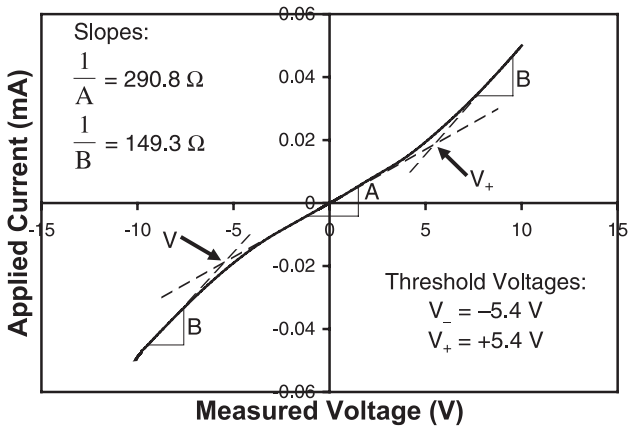

Fig. 1. Current–voltage plot for OPC paste (w/c ratio=0.4) with 1.0 vol.% steel fibers (25.3 mm long, 0.5 mm diameter) at 7 days hydration.

similarly destabilize these oxide coatings, driving electrochemical reactions into active or transpassive corrosion regimes [12]. The present work was aimed at correlating the slopes in $I–V$ plots (e.g., Fig. 1) with features in impedance Nyquist plots, thereby allowing for a better interpretation of the underlying mechanism(s) of nonlinear $I–V$ behavior in cement-based composites.

2. Experimental procedure

Ordinary Portland cement (type I OPC) was mixed by hand with a water-to-cement (w/c) ratio of 0.4 and homogenized in a commercial blender. Macrofibers (0.5 mm diameter) made of steel were cut to three lengths (6.4, 12.6, and 25.3 mm). Appropriate quantities of each fiber-length wire were hand-mixed into cement paste to make up 1.0 vol.% of fibers. At these combinations of aspect ratio and loading, the fibers should not be percolating [13]. These mixes were cast into cylindrical PVC molds (45 mm diameter by 95 mm height). The samples were cured in 100% RH for 7 days, at which point the samples were subjected to impedance and four-point DC resistance measurements.

Aqueous electrodes were constructed for both IS and DC studies. Samples were mounted vertically, as shown in Fig. 2a, with the bottom end slightly submerged in a sodium chloride solution in which a copper mesh electrode was placed. A similar electrode arrangement was mounted at the top end of the specimen, with a sodium chloride solution reservoir and a submerged copper mesh electrode. In each case, the external electrode was no more than 2–3 mm from the end of the specimen. The aqueous electrodes were employed to optimize electrochemical contact with each end of the specimen, which is especially important at high DC currents. Separate studies with only the copper mesh electrodes separated by ~5 mm of sodium chloride solution proved that the resistance due to the external electrolyte was less than 1 Ω, and could be neglected. To limit interdiffusion between the solution in the reservoirs and the pore solution in the specimens, IS measurements were performed as quickly as possible after mounting. Given that the voltage leads in four-point DC measurements are at considerable distance (1–2 cm) from the reservoirs, DC resistance should be unaffected by interdiffusion (or electromigration), at least for the brief time period of measurements (~15 min). Shielded cables connected each electrode to an impedance/gain-phase analyzer (Solartron 1260, Houston, TX). Impedance scans were taken from 11 to 100 MHz with an excitation amplitude of 1 V.

To enable four-point DC resistance measurements, thin steel wires were wrapped tightly around the specimen cylinders at approximately 20% and 80% positions along their lengths. Contact between the wire loops and the sample was ensured by painting a 2-mm wide strip of silver colloidal paste over the wire. The silver paint was then sealed with a layer of clear enamel. Currents between ±50 mA were generated by a constant current source (Keithley 220, Cleveland, OH) and applied through the reservoir electrodes, with voltage drops measured between the two wire loops. Four-point measurements eliminated possible electrode contributions in two-point measurements. In every

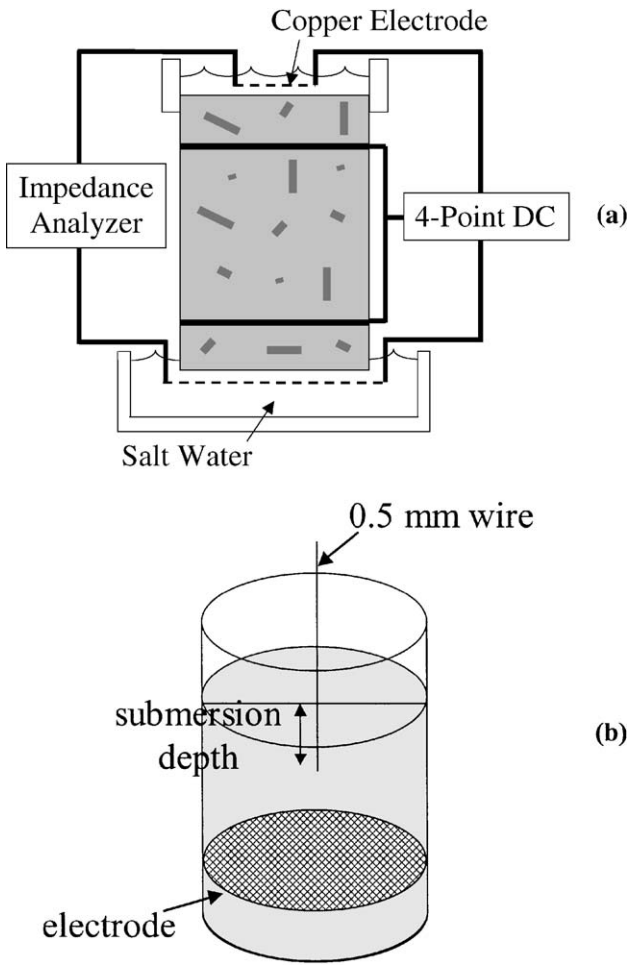

Fig. 2. Experimental setup for (a) impedance and four-point DC resistance measurements and (b) single-wire spreading resistance studies.

case, the four-point DC resistance, when corrected for the difference in interelectrode spacing, agreed with the IS-derived resistance, within experimental uncertainty (±5% for each technique).

Single-wire simulations were carried out in tap water inside a tall glass cylinder (75.7 mm diameter) as shown schematically in Fig. 2b. A copper-mesh electrode was affixed to the bottom of the cylinder and was connected to the impedance analyzer by a shielded cable. A vertically mounted test wire, also connected by shielded cable to the analyzer, served as the other electrode. Its position relative to the copper mesh electrode could be variable or fixed. The diameter of this wire matched that of the fibers used in the composites (0.5 mm). The water level in the cylinder could also be varied to control the extent of submersion of the test wire. As pointed out in previous work, tap water has resistivity/dielectric properties comparable to those of mature cement pastes [5–7] and is therefore useful to simulate the impedance response of fiber-reinforced composites.

3. Results and discussion

Fig. 3 shows typical impedance results for cement–matrix composites with 1.0 vol.% steel fibers, in this case 12.6 mm in length, at 7 days of hydration. Also shown for comparison is the Nyquist plot for fiber-free cement paste at the same age and w/c ratio (0.4). In both cases, there is indication of a much larger low-frequency (high impedance) electrode arc beginning at the right side of each spectrum. Copper-mesh electrodes were employed in the present work, and this arc is attributable to passive oxide film formation on the measurement electrodes [8]; the frequency at the top of this arc is typically in the megahertz range, corresponding to the millifarad range of capacitance associated with electrode films and/or double layers [9].

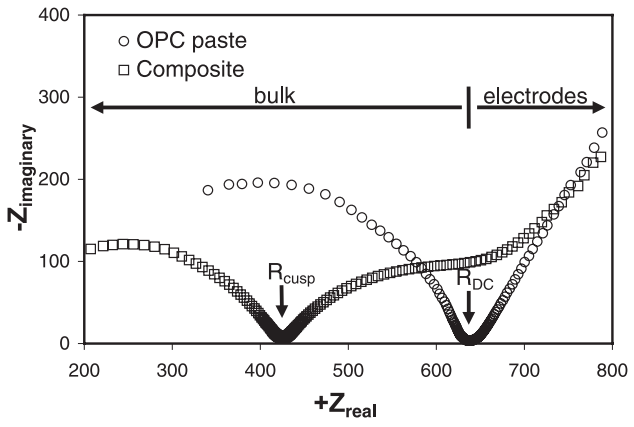

Fig. 3. Typical impedance spectra (Nyquist plots) for OPC paste (w/c ratio=0.4) with and without 1.0 vol.% steel fibers (12.6 mm long, 0.5 mm diameter) at 7 days of hydration. The frequency at the top of the single bulk arc (OPC paste) is the same as for the left (high frequency) bulk arc (composite)—approximately 8 MHz. The frequency at the top of the right (low frequency) bulk arc for the composite is approximately 25 Hz.

Table 1
Comparison of $I-V$ and IS measurements

Material	$I-V$ (Ω)		IS (Ω)	$V_{threshold}$ (V)
	R_{DC}[a]	R_{HI-V}	R_{cusp}	
OPC paste	652.3	–	636.7	–
FRC (6.4-mm fibers)	692.3	N/A	613.9	N/A
FRC (12.6-mm fibers)	696.6	473.3	446.4	10.1
FRC (25.3-mm fibers)	649.5	333.4	303.0	5.4

FRC=fiber-reinforced cement.
[a] Low voltage slope in the $I-V$ plot.

The "bulk" portion of the impedance spectrum is clearly influenced by the presence of fibers. The plain paste exhibits a single bulk arc, whose frequency at the maximum $|Z_{imag}|$ is in the megahertz range (picofarad range of capacitance). The intersection of this arc with the electrode arc consistently agrees with the four-point DC resistance, as shown. Upon the addition of fibers, the bulk arc is subdivided into two subarcs, which intersect at the "cusp frequency" in Fig. 3. The resistance at this point will be referred to as the cusp resistance (R_{cusp}) hereafter. The frequency at the top of the high-frequency (left) arc is virtually identical to that of the plain paste (megahertz range) and is most likely associated with interfiber bulk transport (see Fig. 3). The other arc is somewhat convoluted with the electrode arc, however its maximum $|Z_{imag}|$ can be estimated to occur in the 10- to 100-Hz range (microfarad capacitance range), and is therefore consistent with multiple interface contributions (due to fibers). The bulk/electrode intersection resistance can be obtained by careful deconvolution of the overall impedance spectrum, or the bulk DC resistance can be obtained by separate four-point measurements, as in the present study.

The values of R_{DC} and R_{cusp} (obtained by IS) are given for each of the composites studied in Table 1. Since the interelectrode spacing is different for the two techniques, the DC resistance was appropriately scaled to correspond to the longer interelectrode spacing in the IS measurements. Furthermore, adjustments were made for sample-to-sample differences in cross-sectional area, always normalizing to the geometry of the IS specimens.

$I-V$ plots for each of the specimens are shown in Fig. 4. There was no evidence of nonlinearity in either the plain

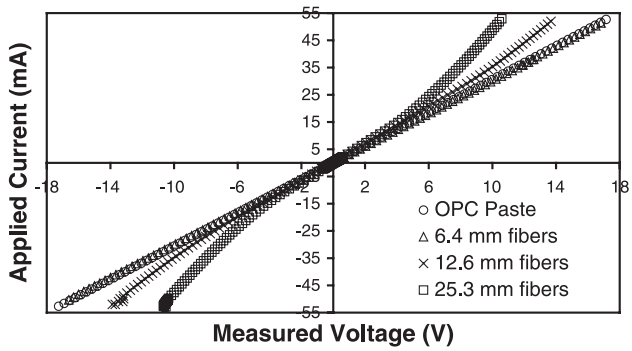

Fig. 4. Current–voltage plots for OPC paste (w/c ratio=0.4) with and without 1.0 vol.% steel fibers at various lengths at 7 days hydration.

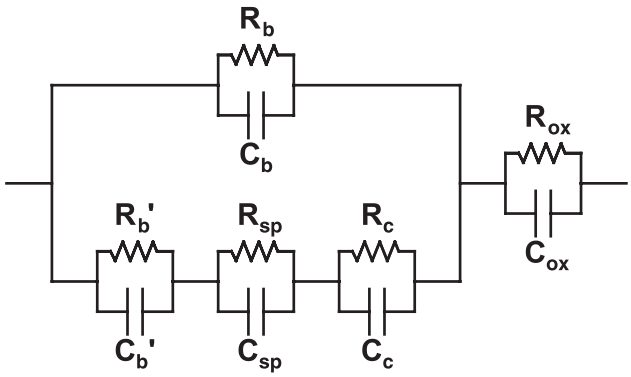

Fig. 5. Equivalent circuit model for conductive fiber-reinforced composites. R=resistor, C=capacitor, b=bulk, sp=spreading, c=coating, ox=oxide. See text for R_b', C_b'.

cement paste or the composite with 6.4-mm-long fibers. However, the composites with 12.6- and 25.3-mm-long fibers showed clear evidence of nonlinearity. Each plot was symmetrical, i.e., the threshold voltage was approximately the same in both directions and the slopes at high field were virtually identical. This can be seen more clearly in Fig. 1. In each case, it was found, within the estimated ±5% uncertainty in each measurement, that the central (low field) slope yielded a resistance in good agreement with the DC resistance from four-point measurements. Similarly, the slope at high field yielded a resistance in good agreement with the cusp resistance from IS measurements, again within ±5% uncertainty in each measurement. The values obtained are given in Table 1.

Both composite behaviors—changeover from high to low resistance upon application of either high frequency or high DC field—can be understood with the aid of the crude equivalent circuit model in Fig. 5 involving various component resistances (R) and capacitances (C). The subscripts stand for bulk (b), spreading (sp), fiber oxide coating (c), and electrode oxide (ox). At low DC fields or low AC frequencies, the fiber oxide coating remains intact. Since R_c is so large, the lower path in the composite is virtually an open circuit; all current is passed through the surrounding bulk, i.e., the upper path (R_b, C_b). Although R_{ox} is similarly large, all current must pass through the excitation electrodes. Therefore, two impedance arcs are obtained for the fiber-free OPC specimen in Fig. 3, one corresponding to the bulk and the other corresponding to the electrodes.

The composite behaves differently, however, with either increasing frequency or increasing DC field. At a critical point, either the "cusp frequency" in IS or the threshold voltage in DC measurements, the oxide coating is no longer blocking for current flow. At high frequencies, displacement currents through the oxide film capacitance (C_{ox}) in Fig. 5 short out the oxide film resistance (R_{ox}), thereby activating the lower conduction path in the equivalent circuit. At high currents, large local fields can drive electrochemical reactions at fiber tips into either active or transpassive corrosion regimes [12], thereby breaching the film resistance (R_{ox}) in Fig. 5. Again, this activates the lower (fiber) conduction path in the equivalent circuit. The fibers become short-circuiting paths through the matrix. At either the cusp resistance or above the threshold voltage, it is fiber-to-fiber bulk transport (and spreading resistance contributions, see below) that govern the lower resistance obtained (R_{cusp} or R_{HI-V}, see Table 1). Since it is still "bulk" in character, albeit of a more localized nature, the time constant (RC product) and characteristic frequency (the frequency at the maximum $|Z_{imag}|$) of the high-frequency (left) arc for the composite in Fig. 3 are identical to those of plain paste.

In the equivalent circuit model of Fig. 5, R_b' stands for the bulk contributions between adjacent fibers and R_{sp} stands for spreading resistance contributions at the fiber tips. Spreading resistance arises due to current-bunching, as originally described by Holm [14]. We previously demonstrated that the spreading resistance of a single fiber tip could be estimated by submerging it at fixed depth in tap water of known conductivity, varying its separation from a large area counter electrode, and measuring the impedance between the two [7]. Fig. 6a shows a plot of cusp resistance (i.e., the intersection between electrode and "bulk" water arcs) vs. electrode separation of a 0.5-mm diameter steel wire at a constant 14 mm submersion in the glass cylinder

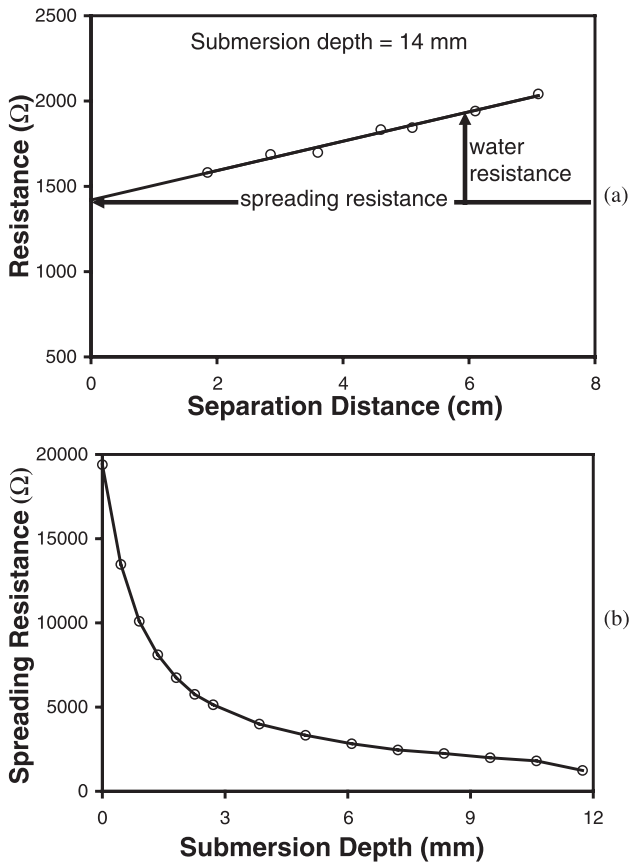

Fig. 6. (a) Measured resistance vs. electrode separation distance at a fixed wire submersion depth of 14 mm. (b) Calculated spreading resistance vs. submersion depth at a fixed separation distance of 11.1 cm.

apparatus of Fig. 2b. The slope of the line corresponds to the increasing resistance of the water column between the two electrodes. The intercept at zero separation is the spreading resistance of the fiber. By similarly separating out the bulk water contributions, the spreading resistance of the fiber at various submersion depths was calculated. This is plotted in Fig. 6b. As expected, there is a rapid falloff in spreading resistance for the first few millimeters of submersion. Expressed in terms of wire diameters, R_{sp} has fallen to ~25% of the initial contact value by ~5 diameters of submersion and to ~10% by ~20 diameters of submersion. Beyond 10 diameters of submersion, the changes in spreading resistance are relatively small. For comparison purposes, the fibers used in the composite work had aspect ratios (length/diameter) of 12.8, 25.2, and 50.6.

Based on the spreading resistance results of Fig. 6, we can now address the variation of threshold voltage vs. fiber length in Fig. 4 and Table 1. The composite with 12.6-mm-long fibers exhibits a threshold voltage nearly double that of the composite with 25.3-mm-long fibers. This can be rationalized with the following thought problem. Consider a single fiber parallel to the applied field direction in a composite. Above the threshold voltage, it acts as a short-circuit element of the microstructure, contributing two spreading resistances in addition to bulk contributions between it and its neighbors (R_b'). Now cut the fiber in half and open a gap between the two halves such that this spacing is approximately the same as between the opposing ends and the adjacent fibers in the composite. Fig. 6b suggests that the spreading resistance at the fiber tips will not be significantly changed as long as the fibers remain 10 or more diameters in length. In our thought problem, the current path above the threshold voltage now involves four as opposed to two spreading resistance contributions (fiber tips) in addition to the relatively unchanged R_b'. Therefore, it is reasonable to expect the threshold voltage to approximately double, i.e., twice as much overall field must be applied to achieve the same threshold value at a given fiber tip. Following the same argument, we would predict a threshold voltage of ~20 V for the composite with 6.4-mm-long fibers. Since the corresponding current level was outside of the experimental range (±50 mA), the transition is not observed in Fig. 4.

The approximately inverse relationship between threshold voltage and fiber length is similar to what is observed in GBC electroceramics. In varistors, for example, the threshold or breakdown voltage is inversely proportional to grain size, being essentially determined by the number of grain boundary barriers in the current path [3]. By halving the grain size, the number of barriers doubles and therefore the breakdown voltage also doubles.

There are important differences, however, between the conductive fiber composites in the present work and typical GBC electroceramics. In GBC electroceramics, the grain boundary barriers are completely blocking at small fields. Once the threshold or breakdown voltage is exceeded, the current can jump by several orders of magnitude to the value limited by the highly conductive grain cores. In the case of conductive fiber composites, the oxide coatings on the fibers are never blocking to current flow through the surrounding matrix. The boost in current (reduction in resistance) above the threshold voltage is comparatively minor, since the current path still involves portions of the matrix (R_b') in Fig. 5.

A second difference has to do with interfacial stability. Both GBC ceramics and conductive fiber-reinforced composites are reversible as long as voltage excursions are of relatively short duration, and return to their prebreakdown condition after the momentary excess voltage is removed. Long-term voltage/current excursions above threshold, however, can have deleterious effects. This is especially true for conductive fiber-reinforced cements, as in the present work. Here such currents can result in permanent interfacial changes due to local electrochemical reactions and the formation of corrosion products.

It should be pointed out that the oxide film-based fiber coating model used to explain the nonlinear $I-V$ behavior and the dual-arc impedance response of steel fiber-reinforced cement–matrix composites is not universally applicable. For example, carbon fiber-reinforced cement–matrix composites are known to exhibit both nonlinear $I-V$ plots [1] and dual-arc impedance spectra [9], yet carbon does not form a passive oxide film. It is conceivable that the double layer that forms in aqueous solutions (i.e., a charge transfer resistance in parallel with a double layer capacitance) can play the role of the frequency- and/or voltage-switchable coating as in the present work. Further work on carbon fiber composites is being conducted and will be reported separately.

4. Conclusions

By comparing four-point DC resistance measurements over a range of applied currents (±50 mA) with IS over a range of frequencies (11–100 MHz) on steel fiber-reinforced cement–matrix composites, it was demonstrated that the two slopes in $I-V$ plots correspond directly to the DC resistance (low-field $I-V$ slope) and the cusp resistance between the two bulk arcs in IS (high-field $I-V$ slope). A model was developed to explain both phenomena. A passive oxide film forms on fiber surfaces under the high pH cement pore solution. With the application of large DC field or high AC frequency excitation, the high impedance oxide coating can be shorted out or breached, resulting in short-circuit current flow via fibers and an overall decrease in composite resistance. There appears to be an inverse correlation between threshold voltage and fiber length, probably due to the change in the number of spreading resistance (fiber tip) contributions along the conduction path. Although this behavior is similar to that of nonlinear electroceramics (e.g., varistors and thermistors), its interfacial stability is not. Due to the electrochemical nature of current transfer at fiber tips,

permanent (corrosion) damage can occur at the fiber–matrix interfaces if above-threshold DC voltages/currents are applied for a long period.

Acknowledgements

This work was supported by the National Science Foundation under grant no. DMR-00-73197 and made use of facilities of the Center for Advanced Cement-Based Materials.

References

[1] A.J. Moulson, J.M. Herbert, Electroceramics: Materials, Properties, Applications, Chapman & Hall, London, 1990.
[2] A.B. Alles, V.R.W. Amarakoon, V.L. Burdick, Positive temperature coefficient of resistivity effect in undoped, atmospherically reduced barium titanate, J. Am. Ceram. Soc. 72 (1) (1989) 148–151.
[3] T.K. Gupta, Application of zinc oxide varistors, J. Am. Ceram. Soc. 73 (7) (1990) 1817–1840.
[4] S. Wen, D.D.L. Chung, Carbon fiber-reinforced cement as a thermistor, Cem. Concr. Res. 29 (6) (1999) 961–965.
[5] J.M. Torrents, T.O. Mason, E.J. Garboczi, Impedance spectra of fiber-reinforced cement-based composites: a modeling approach, Cem. Concr. Res. 30 (4) (2000) 585–592.
[6] J.M. Torrents, T.O. Mason, A. Peled, S. Shah, E.J. Garboczi, Analysis of the impedance spectra of short conductive fiber-reinforced composites, J. Mater. Sci. 36 (16) (2001) 4003–4012.
[7] T.O. Mason, M.A. Campo, A.D. Hixson, L.Y. Woo, Impedance spectroscopy of fiber-reinforced cement composites, Cem. Concr. Compos. 24 (5) (2002) 457–465.
[8] Y. Feng, K.-S. Siow, W.-K. Teo, K.-L. Tan, A.-K. Hsieh, Corrosion mechanisms and products of copper in aqueous solutions at various pH values, Corrosion 53 (5) (1997) 389–398.
[9] S.J. Ford, J.D. Shane, T.O. Mason, Assignment of features in impedance spectra of the cement-paste/steel system, Cem. Concr. Res. 28 (12) (1998) 1737–1751.
[10] B. Beverskog, I. Puigdomenech, Revised Pourbaix diagrams for iron at 25–300 °C, Corros. Sci. 38 (12) (1996) 2121–2135.
[11] B. Beverskog, I. Puigdomenech, Revised Pourbaix diagrams for copper at 25 to 300 °C, J. Electrochem. Soc. 144 (10) (1997) 3476–3483.
[12] K.B. Oldham, J.C. Myland, Fundamentals of Electrochemical Science, Academic Press, San Diego, CA, 1994, p. 351.
[13] A. Celzard, E. McRae, C. Deleuze, M. Dufort, G. Furdin, J.F. Mareche, Critical concentration in percolating systems containing a high-aspect-ratio filler, Phys. Rev. B 53 (10) (1996) 6209–6214.
[14] R. Holm, Electric Contacts: Theory and Application, Springer-Verlag, New York, 1967.